Mechanisms of influence of the Semi-Annual Oscillation on stratospheric sudden warmings

Lesley J. Gray[1] | **Hua Lu[2]** | **Matthew J. Brown[3]** | **Jeff R. Knight[4]** | **Martin B. Andrews[4]**

[1]Department of Physics, National Centre for Atmospheric Science (NCAS), Oxford, UK

[2]British Antarctic Survey, Cambridge, UK

[3]Department of Physics, University of Oxford, Oxford, UK

[4]Met Office Hadley Centre, Exeter, UK

Correspondence
L.J. Gray, Department of Physics, National Centre for Atmospheric Science (NCAS), Oxford, UK.
Email: gray@atm.ox.ac.uk

Abstract

The influence of the Semi-Annual Oscillation (SAO) on the timing and evolution of major sudden stratospheric warmings (SSWs) is examined using the 2008/2009 SSW as the primary case-study. When the zonal winds in both the troposphere and the SAO region of the equatorial upper stratosphere/lower mesosphere are relaxed towards reanalysis fields in the UK Met Office Unified Model, a remarkably accurate representation of the January 2009 SSW is achieved. The accurate timing of the SSW is determined by the SAO zonal wind relaxation. The westerly-to-easterly phase transition of the SAO in the lower mesosphere (0.1–0.5 hPa) is found to be a key factor for this influence. It defines an initial conical-shaped vortex that determines the upward propagation of wave activity and subsequent evolution of wave mean-flow interaction. Internal transient wave reflection in the subtropics and associated wave-induced acceleration of the mean-flow is found to be an important component, strengthening the vortex and thus delaying the onset of the SSW. The sensitivity of SSW timing to the equatorial westerly winds in the lower mesosphere is further explored in the context of all major SSWs during the 1979–2018 period. The timing of SSWs is found to be significantly correlated with the timing of the equinoctial westerly-to-easterly phase transition at 0.3 hPa in early winter ($r = 0.79$). This relationship is discussed in the context of the more widely recognised influence of the quasi-biennial oscillation (QBO). These results suggest that accurate simulation of the timing of SAO phase transitions, as well as knowledge of the QBO phase, is likely to provide additional and extended Northern Hemisphere wintertime seasonal forecast skill.

KEYWORDS

1. tools and methods: dynamic/processes, general circulation model experiments, 2. scale: global, seasonal, 3. physical phenomenon: dynamics, 4. geophysical sphere: atmosphere, stratosphere, teleconnections (AO, NAO, ENSO, SSW)

1 | INTRODUCTION

Sudden Stratospheric Warmings (SSWs) are the prime source of interannual variability in the Arctic winter stratosphere (Baldwin *et al.*, 2018; 2021). The events are characterised by substantial and rapid warming over the polar stratosphere, of the order of tens of degrees in just a few days, accompanied by a reversal of the winds from their usual westerly to easterly direction. Over the past 40 years for which good satellite coverage is available, major SSWs have occurred on average in six out of 10 winters in the Northern Hemisphere (NH) (Charlton and Polvani, 2007; Butler *et al.*, 2017). There is also significant variability on intraseasonal, interannual and decadal time-scales (Holton and Tan, 1980; 1982; Labitzke, 1982; Lu *et al.*, 2008; Dimdore-Miles *et al.*, 2021).

The impact of SSWs on surface weather and the benefits of accurate long-range forecasts are well recognised (Scaife *et al.*, 2005; 2016; Mukougawa *et al.*, 2009; Sigmond *et al.*, 2013; Butler *et al.*, 2016; 2018; Charlton-Perez *et al.*, 2018; Garfinkel *et al.*, 2018; Domeisen *et al.*, 2020). While extended forecasts of SSWs are clearly an important goal, there is still a limited understanding of the processes that influence the timing and vertical extent of SSWs. Current operational predictability of SSWs beyond ∼15 days is very limited (Tripathi *et al.*, 2015; 2016; Baldwin *et al.*, 2021). Predictability is even shorter for split-type SSWs (∼4–9 days) (Ichimaru *et al.*, 2016; Noguchi *et al.*, 2016). Confident predictions are often only possible once the SSW has already commenced in the upper stratosphere/lower mesosphere (USLM) (Ichimaru *et al.*, 2016; Baldwin *et al.*, 2021). Even when an SSW is indicated in the USLM there remains uncertainty about how deep the SSW may penetrate, i.e., whether it will evolve as a minor warming and influence only the USLM region or whether it will develop into a full major warming with anomalies descending into the lower stratosphere to influence the underlying tropospheric weather patterns (Noguchi *et al.*, 2016).

Future advances in our ability to predict SSWs will rely on identifying the factors that precondition wave mean-flow interactions and on improving our understanding of the spatial and temporal evolution of the stratospheric polar vortex. Substantial progress has been made over the past 40 years, using a combination of observational and theoretical studies (Matsuno, 1971; McIntyre, 1982; Baldwin *et al.*, 2021). SSWs are usually initiated in the USLM region (O'Neill and Pope, 1988; Harvey *et al.*, 2002; 2018; Gray *et al.*, 2004; Greer *et al.*, 2013). Greer *et al.* (2013) found that synoptic-scale disturbances in the USLM have preceded every major SSW. They linked the development of USLM disturbances to the instability of ageostrophic flow and wave breaking, but exactly how USLM disturbances precondition the flow and lead to the development of SSWs remain poorly understood. Observational studies of SSWs have primarily employed reanalysis datasets (Fujiwara *et al.*, 2017) that rely on satellite observations as the prime source of data above ∼10 hPa. However, there remains significant uncertainty in the accuracy of the reanalysis data in the USLM region, where vertical variations of the flow are particularly challenging to determine from the predominantly nadir-sounding observations (SPARC S-RIP, 2022, chapters 9, 11).

The influence of the equatorial stratosphere on SSWs has been studied for many years because of the observed relationship between SSWs and the quasi-biennial oscillation (QBO: Holton and Tan, 1980; 1982). The QBO determines the equatorial winds in the lower to middle stratosphere (10–50 hPa) and thus defines the lower stratospheric waveguide for planetary-scale waves to propagate into the stratosphere and influences the subsequent wave mean-flow interaction near the polar vortex edge (Baldwin *et al.*, 2001; Lu et al., 2014; 2021a). However, relatively few studies have explored the influence from higher regions in the equatorial USLM (∼0.1–5 hPa) where the Semi-Annual Oscillation (SAO) dominates (Garcia *et al.*, 1997). The available studies (Gray *et al.*, 2001; 2004; 2020; Gray, 2003; Pascoe *et al.*, 2006) generally refer to the fact that vertically propagating planetary waves are deep structures and the SAO determines the location of the zero-wind line encountered by them in the USLM. Although those studies clearly point to an influence from the SAO on the timing of SSW, the exact dynamical processes are yet to be determined.

The primary driver of the westerly stratospheric SAO phases, which are centred around the equinox, is momentum transfer associated with fast Kelvin waves and gravity waves. The primary driver of the easterly phase of the stratospheric SAO centred around the solstice periods, on the other hand, is associated with the cross-equatorial advection of easterlies from the summer to winter hemisphere associated with the Brewer–Dobson circulation (Garcia *et al.*, 1997; Smith *et al.*, 2017). Barotropic instability of the subtropical easterly jet in the summer hemisphere also affects the equatorial winds and temperatures in the height region (0.1–5 hPa) where the SAO dominates and its relationship with the 2-day waves has been studied extensively (Salby, 1981; Plumb, 1983; Limpasuvan and Leovy, 1995; Orsolini *et al.*, 1997). Shuckburgh *et al.* (2001) showed that barotropic instability is enhanced, with associated synoptic-scale wave activity, on the flanks of equatorial westerlies (their study examined barotropic instability in the lower stratosphere associated with the QBO, but is also relevant to the USLM). Hitchman and Huesmann (2007) proposed that localized, synoptic-scale wave breaking in the equatorial USLM acts to constrain the growth and breaking of quasi-stationary planetary-scale

waves as well as to prevent them entering the summer hemisphere.

The time-varying nature of the SAO zonal winds is known to induce a secondary meridional circulation in equatorial/subtropical latitudes so that thermal wind balance may be maintained (Gray and Pyle, 1986; Hitchman and Leovy, 1986). Relative downwelling (upwelling) over the Equator is associated with the westerly (easterly) SAO phase, with corresponding ascent (descent) in the subtropics of each hemisphere. This secondary circulation interacts with, and thus influences, the evolution of the larger-scale Brewer–Dobson circulation (Semeniuk and Shepherd, 2001). In general, the westerly phase of the SAO is found to enhance the cross-equatorial flow in the upper stratosphere at ∼3–5 hPa while the easterly SAO phase enhances the cross-equatorial flow in the lower mesosphere (Hitchman and Leovy, 1986). The westerly SAO tends to work together with the westerly phase of the QBO at 50 hPa and their combined effect enhances nonlinear wave breaking in the winter hemisphere (Lu *et al.*, 2021a).

The January 2009 major SSW was a dramatic event and has been used extensively as a case study to examine dynamical processes associated with split-type SSWs (Labitzke and Kunze, 2009; Manney *et al.*, 2009; Harada *et al.*, 2010; Ayarzagüena *et al.*, 2011; Albers and Birner, 2014; Noguchi *et al.*, 2016; Schneidereit *et al.*, 2017; Domeisen *et al.*, 2018; Song *et al.*, 2020). The majority of these studies start their analyses from December or 10–20 days before the event, with a focus on either tropospheric precursors or wave mean-flow interactions in the extratropical winter hemisphere that occur just before the SSW event. However, a recent study of the 2009 SSW examined the sensitivity to early-winter conditions and confirmed an influence from the early-winter SAO region (Gray *et al.*, 2020; hereafter G2020). The study used a state-of-the-art seasonal forecast model to examine the 2008/2009 winter evolution by relaxing the zonal winds in various parts of the atmosphere towards reanalysis fields. They found that the SAO region influenced the timing and vertical extent of the SSW. When the modelled equatorial zonal winds were relaxed towards ERA-Interim (ERA-I) values in the equatorial USLM (between ±10° latitude and above the 5 hPa level) they achieved an accurate simulation of the polar vortex winter evolution, including the January 2009 SSW event. Without the imposed SAO relaxation, the model had an easterly bias in the equatorial USLM, in common with most other models, that prevented the correct evolution of precursor wave mean-flow interactions.

While G2020 demonstrated the importance of the early winter SAO evolution, further insight is required to understand the underlying processes that yield a

successful simulation of the SSW. In this study, we extend the study of G2020 by examining in more detail the early-winter flow development and the associated dynamics, to achieve a better understanding of the mechanisms of SAO influence on SSW timing. We additionally expand their study to explore the potential for extended NH wintertime seasonal forecast skill by examining the sensitivity to the SAO of all major SSWs between 1979 and 2018. The methodology of the study is provided in Section 2. Results are provided in Section 3 and summarised in Section 4.

2 | METHODOLOGY

2.1 | Experimental set-up

Two model experiments from the G2020 study are analysed in this article. They were performed as part of a series of experiments to investigate various factors that may influence the timing of SSWs, including the role of tropospheric planetary wave forcing and the role of an accurately simulated SAO. A description of all the model simulations is provided in G2020, together with an initial analysis of the results. In this article, two experiments (AllTrop and AllTrop-UpStrat-Eq) are analysed in more detail to provide added insight into how the imposed SAO evolution influences the timing of the SSW. The only difference between the two experiments is a relaxation of the zonal winds in the SAO region. In both simulations the tropospheric zonal winds were relaxed throughout the winter towards 6-hourly fields from the European Centre for Medium-Range Weather Forecasts (ECMWF) ERA-Interim reanalysis (ERA-I; https://www.ecmwf.int/en/forecasts/datasets/reanalysis-datasets/era-interim). In the AllTrop-UpStrat-Eq simulation the zonal winds were additionally relaxed in the region of the SAO. Details of the relaxation region and method are provided below. The simulations were performed using the atmosphere-only configuration of the Met Office Unified Model (UM, GA7.0 version 10.3: Walters *et al.*, 2019) at N96 resolution (∼1.25° latitude, 1.875° longitude) and with 85 vertical levels extending to 85 km (0.0053 hPa). Fifty-member ensembles were performed for each experiment.

Both experiments were initialised with ERA-I zonal and meridional wind and temperature fields on 1 September 2008 and then allowed to evolve freely through to April 2009, except in the selected regions where they were relaxed towards the corresponding ERA-I data (see below). The correct phase of the QBO was achieved by the initialisation, and a realistic QBO evolution through to April was achieved in both simulations through the non-orographic gravity-wave parametrization scheme (Walters *et al.*, 2019).

The relaxation of the zonal wind field at each time step used a Newtonian scheme

$$\Delta X = G\Delta t \,(\text{Xanalysis} - \text{Xmodel})$$

where X denotes the field, ΔX is the increment applied over the time interval Δt and G is the relaxation parameter (a constant). A 6-hour relaxation time-scale was employed (Telford *et al.*, 2008). The relaxation was applied only above 2.5 km to avoid the atmospheric boundary layer. A linear tapering to zero was applied over two model levels above and below the specified height to avoid abrupt changes at the edge of the relaxation region (the resulting tapering extended between 1 and 5 km depending on the height region since the vertical model spacing is not uniform). In both experiments the zonal wind field relaxation was applied from 2.5 km up to the tropopause, identified by the closest model level to the local lapse-rate tropopause. Note that this is slightly different to G2020 which relaxed zonal winds, meridional winds and temperature in the troposphere. In this study we have only relaxed the zonal winds. Removing the relaxation of meridional winds and temperatures in the troposphere had virtually no impact on the SSW evolution and thus was not considered to be necessary. In the AllTrop-UpStrat-Eq experiment the zonal winds were additionally relaxed towards ERA-I fields in the equatorial upper stratosphere between 10°S and 10°N and above the 5 hPa level (with linear tapering to zero by ±15°). The paucity of observations means that there is relatively large uncertainty in the veracity of the ERA-I data in the equatorial USLM region and substantial disagreement exists between different reanalysis datasets (SPARC S-RIP, 2022, chapter 11). Nevertheless, the results of G2020 demonstrate that relaxation of the model towards the ERA-I data in this region enables a substantially improved simulation of the polar vortex evolution, suggesting that the relaxation towards ERA-I reanalysis fields eliminates an important model bias.

As described in G2020, the experiments were performed as 50-member ensembles. All diagnostics presented in the article are taken from the first ensemble member of the relevant experiment, as a representative of the whole ensemble. In the AllTrop-UpStrat-Eq experiment the ensemble members followed nearly identical trajectories (see G2020 figure 1b), so the first ensemble member is almost identical to the ensemble-average. In the AllTrop experiment there was more variability (see G2020 figure 1a) but the overall nature and timing of the vortex variations were very similar and none diverged more than 10 days from the ensemble mean. However, the aim of the article is to understand SSW mechanisms involving individual wave events and their interactions. We therefore choose to show results from a single representative ensemble member rather than the ensemble-mean to avoid loss of accuracy due to smoothing associated with small mismatches in the timing of wave events. We use the same ensemble member from each experiment to ensure that the initial conditions are identical.

2.2 | Wave driving diagnostics

Eliassen–Palm (E-P) fluxes $\bar{\mathbf{F}} = (F^{(\phi)}, F^{(z)})$ are used to indicate Rossby wave propagation and the E-P flux divergence (EPFD hereafter) measures the wave forcing, or body drag on the zonal mean-flow (Andrews *et al.*, 1987). In spherical pressure coordinates EPFD takes the form

$$\nabla \cdot \mathbf{F} = \frac{1}{a\cos\phi} \left[F^{(\phi)} \cos\phi \right]_\phi + F_z^{(z)}, \qquad (1)$$

where the meridional and vertical components of the E-P fluxes $F^{(\phi)}$ and $F^{(z)}$ are

$$F^{(\phi)} = \rho_0 a \cos\phi \left(\frac{\overline{v'\theta'}}{\theta_z} \overline{u}_z - \overline{v'u'} \right)$$

$$F^{(z)} = \rho_0 a \cos\phi \left\{ \left[f - \frac{1}{a\cos\phi}(\overline{u}\cos\phi)_\phi \right] \frac{\overline{v'\theta'}}{\theta_z} - \overline{w'u'} \right\}, \qquad (2)$$

where a is the mean radius of the Earth, f is the Coriolis parameter, z is the log-pressure height, ϕ is latitude, θ is the potential temperature, ρ_0 is the basic density, u, v and w are the zonal, meridional and vertical velocities. The overbar, prime and subscript denote zonal average, departures from zonal average, and derivative, respectively.

The calculations of $F^{(\phi)}$, $F^{(z)}$ and $\nabla \cdot \mathbf{F}$ were carried out using 6-hourly model data. The fields were further separated into stationary and transient contributions. The stationary component was calculated by applying a 31-day centred averaging window to the relevant variables at each grid point. The transient component was estimated by taking the difference between the instantaneous 6-hourly field and the stationary component at that time. The contributions from a selected range of zonal wave numbers were also estimated by applying a Fast Fourier transform filter longitudinally to the relevant variable with the required zonal wave numbers before the E-P fluxes and EPFD fields were calculated.

The plotted EPFD was divided by $\rho_0 a \cos\phi$, so that the wave driving term in the transformed Eulerian-mean (TEM) momentum equation has the same units as the zonal wind tendency, that is, $\text{m·s}^{-1}\text{·day}^{-1}$. The E-P fluxes were scaled by the air density, and the vertical component of the E-P fluxes $F^{(z)}$ was further multiplied by

111, for better visualisation of the wave propagation (see Gray (2003) for further details).

To examine the residual-mean meridional circulation and its interaction with the SAO, the TEM form of meridional and vertical velocity

$$\bar{v}* = \bar{v} - \rho_0^{-1}\left(\rho_0 \overline{v'\theta'}/\overline{\theta_z}\right)_z,\qquad(3)$$

$$\overline{w}* = \overline{w} + (a\ \cos\phi)^{-1}\left(\cos\phi\ \overline{v'\theta'}/\overline{\theta_z}\right)_\phi,\qquad(4)$$

are used to compare the two simulations in terms of cross-equatorial flow and the latitudinal extent of the residual-mean circulation.

2.3 | Waveguide and breaking diagnostics

In this study, we use polar stereographic projections of Ertel's PV gradient on isentropic theta surfaces (P_ϕ) to examine planetary-scale waveguides and wave breaking. They are also used to identify the edge of the stratospheric polar vortex by locating steep meridional gradients and to identify regions where $P_\phi \leq 0$, indicating wave breaking/absorption, which are commonly found in the surf zone and near the subtropical zero wind line.

In addition, latitude–height cross-sections of quasi-geostrophic potential vorticity gradient ($\overline{q}_\phi$) are plotted together with TEM meridional circulation $\bar{v}*$ and $\overline{w}*$ (see Equations 3 and 4) to examine the link between wave breaking and the outflow from the equatorial USLM associated with the residual mean circulation. $\overline{q}_\phi$ is calculated as

$$\overline{q}_\phi = 2\Omega\cos\phi - \left[\frac{(\overline{u}\cos\phi)_\phi}{a\cos\phi}\right]_\phi + \frac{af^2}{N^2}\left(\frac{\overline{u}_z}{H} - \overline{u}_{zz}\right),\quad(5)$$

where Ω is the Earth's angular velocity, H is the mean scale height (7 km), N is the buoyancy frequency, and a is the Earth's radius.

3 | RESULTS

In this section we compare the evolution of the two simulations. The AllTrop-UpStrat-Eq simulation successfully reproduces the timing of the January 2009 SSW (and is hereafter referred to as the successful simulation) while the AllTrop simulation fails (and is hereafter referred to as the failed simulation). The only difference between the simulations is the relaxation of zonal winds in the SAO region (above 5 hPa, 10°S–10°N) in the successful

simulation. We concentrate on the autumn and early winter period as the vortex begins to develop, to better understand why the additional relaxation of zonal winds in the equatorial USLM of the successful simulation preconditions the vortex and is so influential in determining the timing of the 2008/2009 SSW (Section 3.1). We then go on to examine whether the improved understanding of the 2009 SSW can be applied more generally to the entire period 1979–2018 for which USLM data are available, to predict the likelihood and timing of a major SSW.

3.1 | Early winter influence of the SAO

The time evolution of the daily zonally averaged zonal winds at 60°N for the 2008/2009 successful simulation is shown in Figure 1a (red contours). As shown in G2020, this time evolution is almost identical to the ERA-I evolution for that winter, including the timing of the SSW in late January and its vertical structure. The zonal winds strengthen throughout the winter reaching a maximum of $\sim$70 m·s^{-1} in mid-January, followed by a dramatic reduction and reversal of the winds at the time of the SSW on 24 January, in excellent agreement with the observed winter evolution. The daily total EPFD averaged over 45–75°N are superimposed (colour shading), to indicate the time evolution of wave mean-flow interaction. Sporadic negative EPFD (blue shading), for example around 10 December, indicates the occurrence of Rossby wave breaking and absorption when easterly wave momentum is transferred from the wave to the zonal flow causing a corresponding sporadic weakening of the vortex. However, from mid-December, periods of positive EPFD are evident, implying wave-induced acceleration of the mean-flow. During the same period, the vortex indeed grows in strength and extends deeper into the lower stratosphere until a large burst of negative EPFD in mid-January gives rise to the SSW.

The prolonged period with eddy-induced acceleration of the polar vortex indicates that eddy momentum convergence, which is associated with the horizontal component of EP fluxes and normally of the opposite sign to eddy heat flux convergence, must play an important role during this period. A number of observational studies (e.g. Hartmann *et al.*, 1984; Mechoso *et al.*, 1985) have noted the presence of regions of positive EPFD, especially in the high-latitude upper stratosphere. Robinson (1986) suggested that some of these high-latitude positive EPFD values may be spurious. However, the periods of positive EPFD shown in Figure 1a appear to be realistic, since they correlate well with periods of zonal wind acceleration (a similar effect was found by Hartmann *et al.* (1984) and discussed further by Andrews (1987)).

(a)

(b)
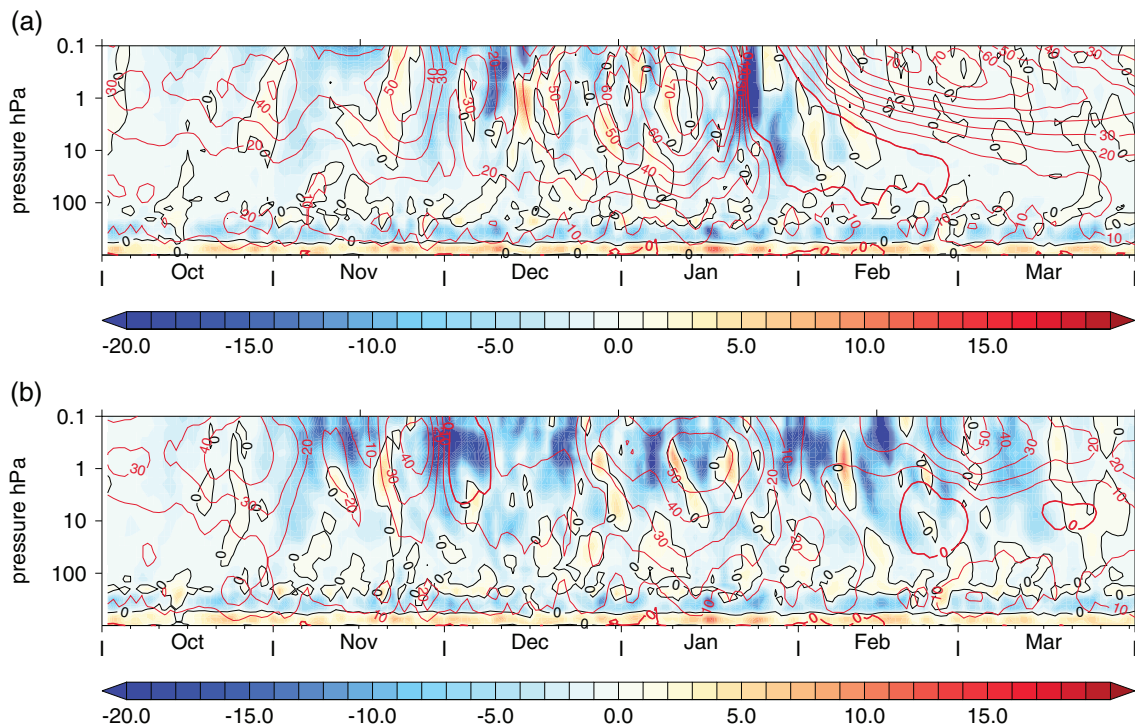
FIGURE 1 Time-series (2008-2009)/pressure (hPa) of zonally averaged zonal winds at 60°N (red contours; m·s^{-1}; thick contour indicates the zero-wind contour) and E-P flux divergence (shaded; m·s^{-1}·day^{-1}) averaged over 45–75°N from (a) the successful (AllTrop-UpStrat-Eq) simulation in which the zonal winds were relaxed in the upper equatorial stratosphere as well as in the troposphere, and (b) the unsuccessful (AllTrop) simulation in which the zonal winds were relaxed only in the troposphere [Colour figure can be viewed at wileyonlinelibrary.com]

In the failed simulation (Figure 1b) the evolution shows stronger, concurrent wave absorption and polar vortex deceleration, particularly in the height range between 1 hPa and 0.1 hPa. Episodes of negative EPFD are evident from early November and the zonal winds at 60°N remain relatively weak throughout the winter. In late November the wave forcing is sufficient to cause the reversal of winds to easterly in the USLM, as shown by the thick red zero wind contour between 5 hPa and 0.1 hPa, 2–6 December, indicating the presence of a minor SSW. Thereafter, the zonal winds remain weaker than in the successful simulation. Despite the relatively strong wave forcing in the failed simulation, a major SSW is not achieved until late February, nearly a month later than observed. Both the December minor warming and the February SSW also failed to reproduce the vertical extent and spatial characteristics of the warming. Both events were characterized by a displaced (wave-1) warming instead of the observed split (wave-2) SSW (not shown).

Although the zonal winds in the successful simulation were only relaxed towards ERA-I in the region above 5 hPa and between ±10° latitudes, the impact of the relaxation spreads to high latitudes and to lower levels once Rossby waves begin to propagate vertically from the troposphere in early winter. Figure 2 shows the early

winter monthly-averaged latitude–height distributions of zonally averaged zonal winds in the ERA-I reanalysis and the two simulations from September through to December. By experimental design both simulations are nearly identical to the ERA-I fields below 5 hPa at equatorial latitudes (and also in the troposphere at all latitudes, not shown). By November/December the polar vortex amplitude and shape in the two simulations are substantially different.

At equatorial latitudes the main differences between the two simulations as a result of the relaxation are not found at 1–3 hPa where the SAO amplitude is greatest, but on the upper flank of the SAO in the lower mesosphere (LM) between 0.1 and 0.5 hPa (see also G2020 figure 3). Without any relaxation, a "nose" of equatorial easterlies develops in the failed simulation from October through to December above 0.5 hPa (Figure 2c). It extends from the summer hemisphere across the equatorial latitudes and reaches as far north as ∼20°N in December. These equatorial easterlies are very weak in September, but they strengthen with time and descend, reaching in excess of 30 m·s^{-1} by December at ∼0.5 hPa. In contrast, the successful simulation (relaxed towards the ERA-I winds in the equatorial USLM and hence identical to the ERA-I reanalyses in this equatorial region) remains westerly above 0.5 hPa until mid-November (Figure 2b). Thus,
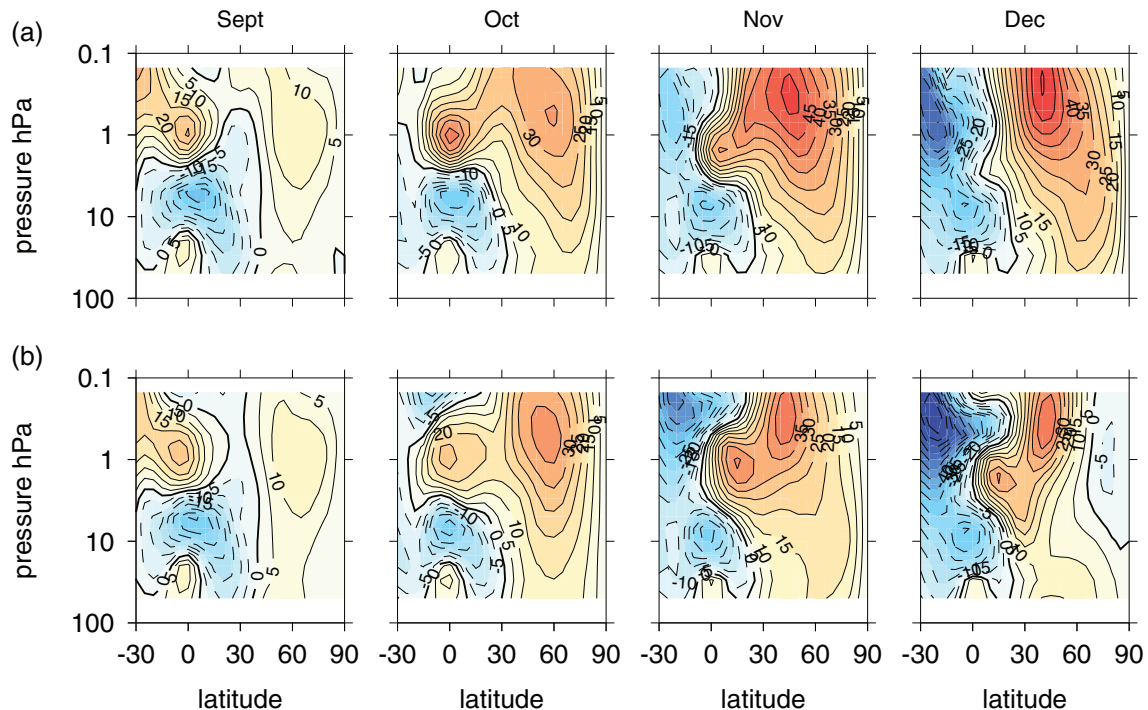
FIGURE 2   Latitude–height cross-sections of monthly-averaged, NH zonally averaged zonal winds (m·s⁻¹) from (a) the ERA-I reanalysis dataset, (b) the successful AllTrop-UpStrat-Eq simulation and (c) the unsuccessful AllTrop simulation. Easterly winds are denoted by dashed contours [Colour figure can be viewed at wileyonlinelibrary.com]

without the imposed relaxation, the model develops an easterly phase of the SAO too early in the LM. G2020 noted the easterly bias of the model (see their figure 3) which is also a common bias among climate models (Smith *et al.*, 2017; 2020).

The differences in the USLM winds at equatorial latitudes are accompanied by distinctly different developments of the polar vortex in the NH. In the successful simulation, the relaxation of the SAO in the USLM delays the northward movement of the zero-wind line. From October, the polar vortex axis starts to tilt equatorward as height increases, in good agreement with the ERA-I reanalyses. The polar vortex from October to December is characterized by a wide, conical-shaped geometry that is narrow in the mid-to-lower stratosphere but wide in the USLM. Waugh and Dritschel (1999) used an idealised model configuration to study the dependence of Rossby wave propagation and subsequent breaking on the initial shape of the vortex. They found that upward propagation of wave activity is inhibited if the polar vortex area increases with height (as in the successful simulation and the ERA-I reanalyses) compared to a cylindrical vortex where the area remains constant with height (more like in the failed simulation). A recent reanalysis-based study also found that wave breaking and the vertical penetration of the stratospheric polar vortex into the lower stratosphere in mid-to-late winter are both affected by the shape of the early winter polar

vortex near the stratopause (Lu *et al.*, 2021b). A strong conical-shaped vortex geometry has also previously been identified as an important precondition for split SSWs (Albers and Birner, 2014). Our results are consistent with these studies.

The broader vortex in the USLM in early winter of the successful simulation is less susceptible to disturbances from the troposphere than in the unsuccessful simulation, as we have already seen in Figure 1. Indeed, from November the polar vortex of the successful simulation strengthens and extends downward. In contrast, in the failed simulation the USLM zero-wind line moves relatively rapidly from the subtropical summer hemisphere into the subtropical winter hemisphere from October, reaching as far north as ~20°N by December. The upper-level polar vortex is thus noticeably narrower from October onwards. The resulting narrow upper-level waveguide acts to confine the wave activity closer to the polar vortex. This early containment of wave activity to the high latitudes leads to a weaker polar night jet throughout the stratosphere, with an unrealistic orientation of the jet in the midlatitude USLM that slopes poleward as height increases.

To better appreciate the differences in the early-winter waveguide between the two simulations, Figure 3a,b show the October averaged meridional gradient of Ertel potential vorticity (P_ϕ; colour shading) on the 2,800 K isentropic level (~0.2 hPa), which is the height of the
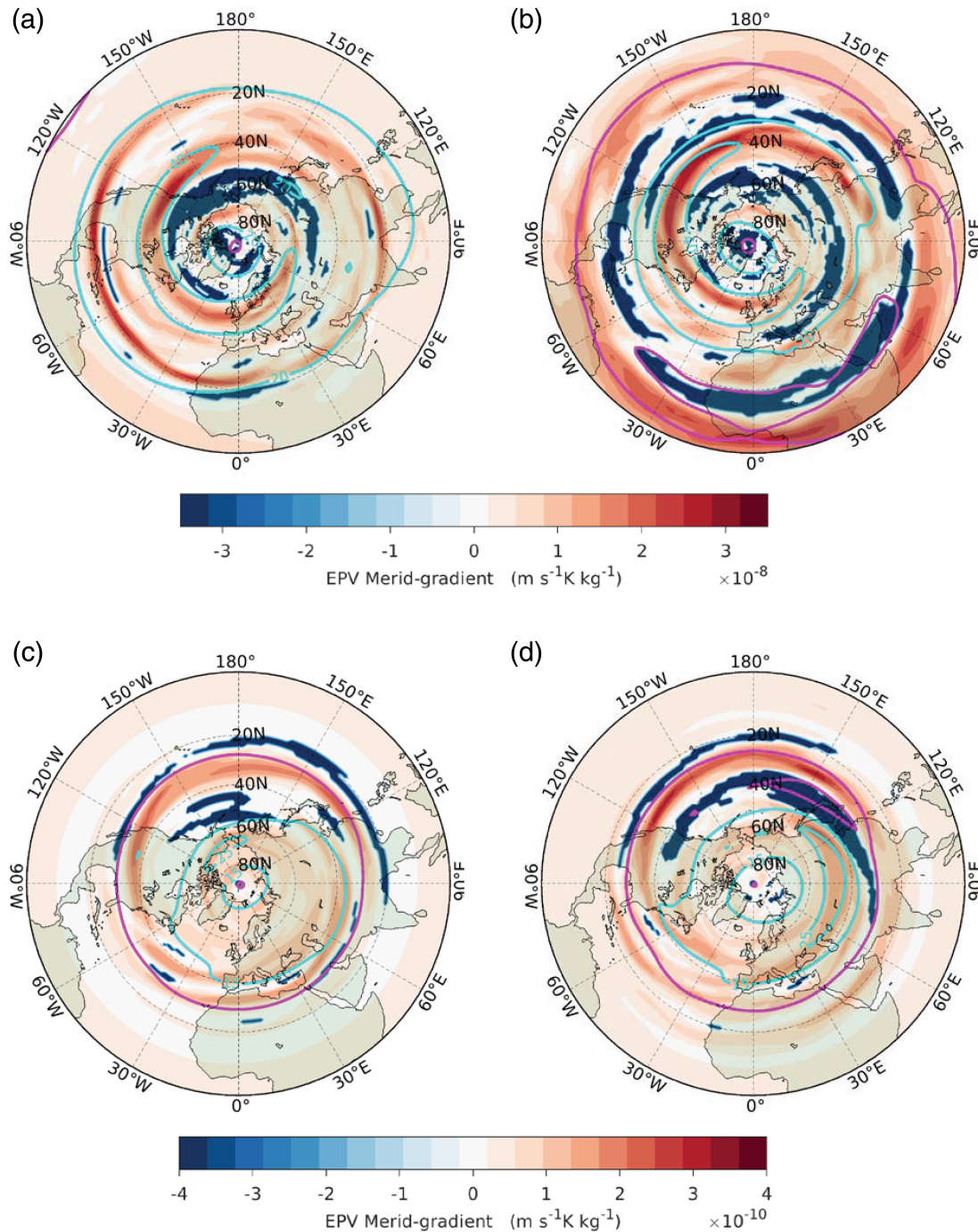
FIGURE 3 October-averaged polar stereographic plots of meridional gradients of Ertel potential vorticity (shaded; m·s⁻¹·K·kg⁻¹). Left panels (a,c) are from the successful (AllTrop-UpStrat-Eq) simulation, right panels (b,d) are from the unsuccessful (AllTrop) simulation. Top panels (a,b) show the 2,800 K surface (~0.2 hPa). Bottom panels (c,d) show the 850 K surface (~10 hPa). Overlaid are the zonal-wind contours (m·s⁻¹; cyan contours with 10 m·s⁻¹ intervals starting at 20 m·s⁻¹; the zero-wind contour is highlighted in magenta) [Colour figure can be viewed at wileyonlinelibrary.com]

equatorial easterly nose in the unsuccessful simulation (Figure 2c). The polar vortex edge is indicated by the cyan contours showing zonal wind speed. In the successful simulation, the zero-wind line (magenta contour) is absent in the NH and the vortex winds broaden into the subtropics, indicated by the 20 m·s⁻¹ zonal wind contour at

20°N (Figure 3a). Wave breaking and mixing occurs primarily on the poleward flank of the vortex, as evident from the regions with $P_\phi \leq 0$ north of ~50°N (dark blue shading). In contrast, the zero-wind contour appears at ~10°N in the AllTrop simulation (Figure 3b), corresponding to the northward edge of the easterly nose near 0.2 hPa
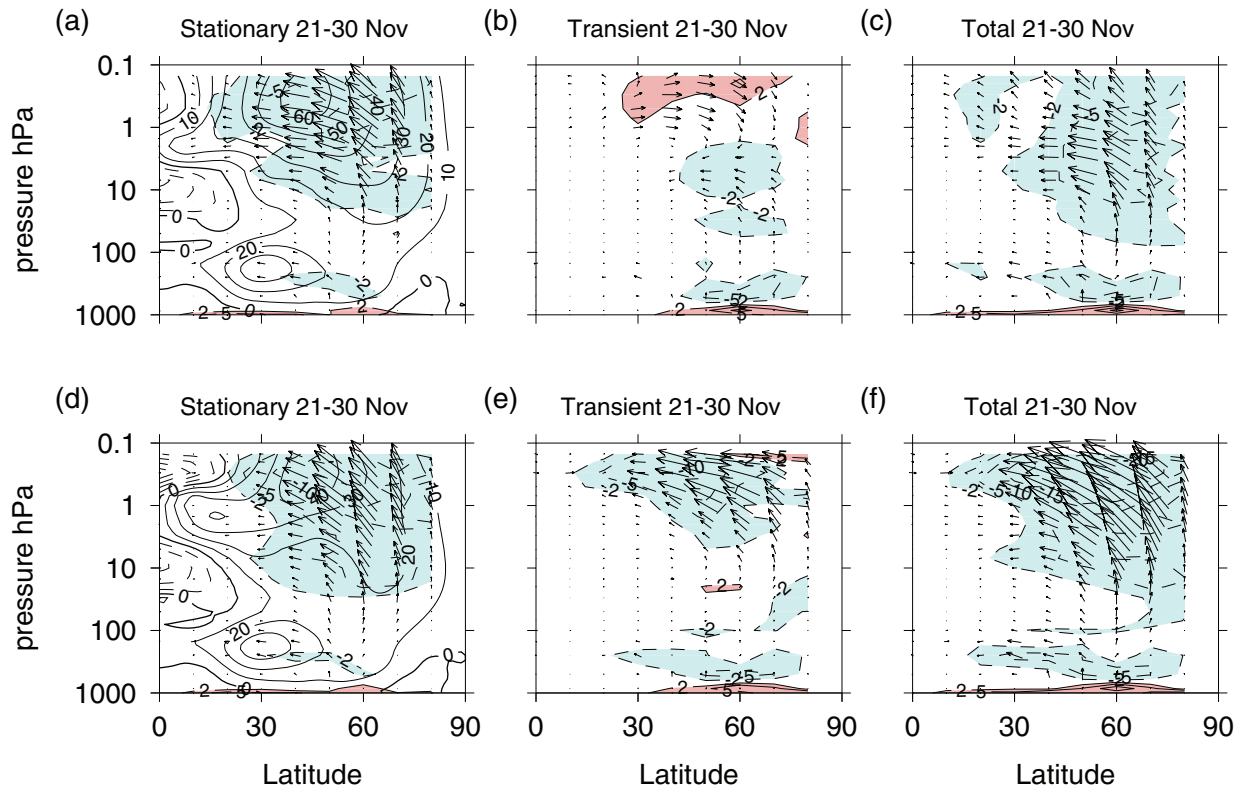
FIGURE 4 November 21st–30th 2008 averaged latitude–height cross-sections showing stationary, transient and total EP flux vectors and divergence (m·s^{-1}·day^{-1}; contour interval of 5 m·s^{-1}·day^{-1}) from (a–c) the successful (AllTrop-UpStrat-Eq) simulation and (d–f) the unsuccessful (AllTrop) simulation. Regions of positive EPFD (divergence) are shaded pink, regions of negative EPFD (convergence) are shaded blue. Contours of the zonal winds are overlaid on the stationary components to show the position of the vortex (m·s^{-1}; thick black line is zero) [Colour figure can be viewed at wileyonlinelibrary.com]

in Figure 2d. Substantial regions with $P_\phi \leq 0$ are found on the poleward side of the zero-wind line and the effect swirls poleward along the polar vortex edge. They indicate wide-spread overturning EPV contours, consistent with repeated occurrences of large E-P flux convergence in the extratropical USLM (Figure 1b).

Figure 3c,d show the corresponding distributions on the 850 K surface (~10 hPa). Regions of negative $\overline{P}_\phi$ are mostly confined to the Aleutian High over the North Pacific sector in both simulations. However, the area of negative $\overline{P}_\phi$ is noticeably smaller in the successful simulation (Figure 3c) than in the failed simulation (Figure 3d). The results indicate that even though the stratospheric zonal wind relaxation in the successful simulation is applied only in the equatorial USLM, by October the wave mean-flow interaction in the mid–high latitude winter stratosphere is already substantially less than in the failed simulation. As a consequence, the polar vortex continues to strengthen in subsequent months (Figure 2).

EP-flux diagnostics provide supporting evidence for the differences in wave forcing and the influence of the SAO winds. G2020 examined the differences between monthly-averaged E-P fluxes and EPFD from the two

simulations (see their Figures 3 and S4). As a further example, Figure 4 shows the E-P fluxes and associated EPFD averaged over the 10-day period 21–30 November, just before the early December minor SSW that occurs in the failed simulation (Figure 1). In both simulations, the stationary and total E-P fluxes point upward and are refracted equatorward towards the critical surface near the zero-wind line in the subtropics. The USLM zero-wind line in the successful simulation is positioned near 10°N, allowing the stationary Rossby waves to propagate deeper into the equatorial region (Figure 4a) than in the failed simulation where it is positioned near 20°N (Figure 4d). The corresponding regions of E-P flux convergence (blue shaded) are found mainly in the extratropics and along the polar vortex edge.

Major differences between the E-P fluxes in these two simulations are evident primarily in the transient components. In the successful simulation the equatorward extended stationary E-P fluxes in the USLM are accompanied by poleward-pointing transient E-P fluxes above 5 hPa near 25–40°N and downward-pointing transient E-P fluxes at high latitudes (55–75°N; Figure 4b). Near the subtropical zero-wind line ($\overline{u} = 0$), incident

quasi-stationary planetary-scale Rossby waves from the extratropical winter hemisphere can be either absorbed or reflected depending on the amplitude of the incident waves and the stage of wave mean-flow interaction (Killworth and McIntyre, 1985; Brunet and Haynes, 1996; Walker and Magnusdottir, 2003). The poleward- and downward-pointing E-P fluxes arrows shown in Figure 4b suggest internal transient wave reflection. They also imply wave-induced acceleration of the mean-flow, in contrast to the more common distribution of E-P flux arrows that point upward and equatorward, implying wave-induced deceleration of the mean-flow. The net effect of the stationary and transient waves in the successful simulation is thus a relatively small peak value of total EPFD (-5 m·s^{-1}·day^{-1}) in the region of the polar vortex edge between 50 and 70°N in the USLM.

In contrast, there is no evidence of poleward and downward reflection of transient waves in the failed simulation (Figure 4e). The E-P fluxes of both stationary and transient waves point upward and equatorward and converge strongly in the USLM (Figure 4d,e). The net effect of stationary and transient waves is a much stronger total wave forcing on the upper-level polar vortex, with a peak value of EPFD of nearly -25 m·s^{-1}·day^{-1} at 55°N, 0.3 hPa (Figure 4f), which is nearly five times greater than in the successful simulation. This strong wave forcing of the polar vortex in the failed simulation leads to the minor warming in early December, in which the zonally averaged zonal winds turn to easterly above 5 hPa at 60°N (Figures 1 and 2h). In contrast, the successful simulation shows a strengthening of the winds from ~20 m·s^{-1} at 1 hPa at the end of November to 40 m·s^{-1} by early December.

These differences in early-winter wave forcing suggest that the SAO westerly phase in the USLM has impacted not only the upper-level vortex shape but also the nature of wave mean-flow interactions throughout the entire winter stratosphere. The broader vortex of the successful simulation is not only less susceptible to disturbances from the troposphere, thus allowing the vortex to continue to strengthen radiatively, but also the evidence from Figure 4 suggests that poleward reflection of transient waves from the subtropics actually contributes to the strengthening of the vortex. Comparison of the stationary EPFD components in Figure 4 indicates that they reach -15 m·s^{-1}·day^{-1} in the failed simulation but only -5 m·s^{-1}·day^{-1} in the successful simulation, a factor of three difference. This suggests that the reflected finite-amplitude transient waves may act to suppress the baroclinic growth of quasi-stationary waves from below. One contributing factor for this could be that the reflected transient anticyclones from the USLM subtropics in the successful simulation grow to finite-amplitude as they spiral in around the edge of the vortex (O'Neill and Pope, 1988; Harvey *et al.*, 2002; Gray, 2003) and disrupt the waveguide for slowly varying quasi-stationary waves from the troposphere. Additionally, as the vortex continues to strengthen and deepen, the increased barotropic shear at the edge of the vortex may hinder the baroclinic growth of quasi-stationary waves, through the "barotropic-control" discussed by James and Gray (1986) and developed further by James (1987).

A sustained contribution of internal reflection of transient waves to the strengthening of the vortex is confirmed by Figure 5. It shows the daily time series of transient wave-2 vertical E-P flux component $F^{(z)}$ from the successful simulation which was found to be a dominant influence in the period leading up to the January 2009 SSW (Albers and Birner, 2014). This figure compares well with the corresponding diagnostic from the JRA25 reanalysis (see figure 10b of Albers and Birner (2014) but note that they did not plot negative values). A series of intervals with negative values of wave-2 $F^{(z)}$ is evident. This effect commences around 21 November (that corresponds to Figure 4b). Following the negative wave-2 $F^{(z)}$ around 21 November there is
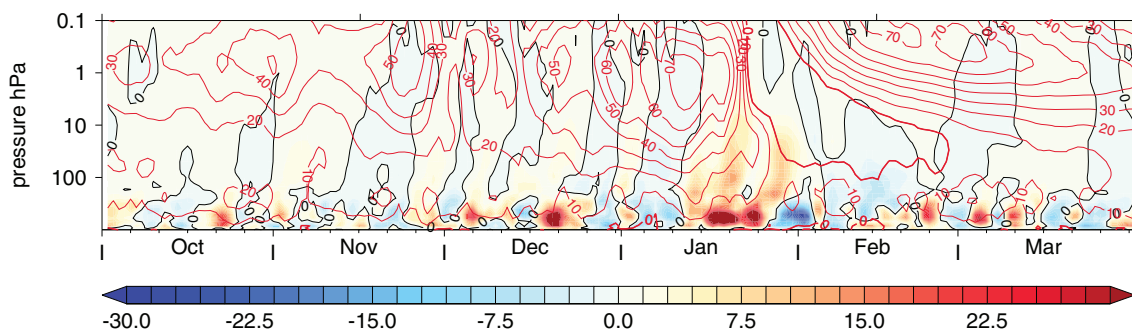

FIGURE 5 Time-series (2008-2009)/pressure (hPa) of transient wave-2 vertical component of EP flux averaged over 45–75°N (shading; units 1×10^{-7} kg·m^{-1}·s^{-4}) from the successful (AllTrop-UpStrat-Eq) simulation. Overlaid are contours of zonally averaged zonal winds (m·s^{-1}) at 60°N; thick red contour shows the zero-wind contour [Colour figure can be viewed at wileyonlinelibrary.com]

a strengthening of the zonal winds a few days later. This forms part of a series of downward reflection/ propagation of wave-2 events from mid-November through to mid-January, e.g. 20–30 November, 11–15 December, 24–28 December and around 4–14 January, each of which precedes a strengthening of the vortex. Throughout this time, the vortex gradually strengthens at lower and lower heights so that by early January, just before the observed SSW occurs, it extends deep into the lowermost stratosphere where it can be more easily influenced by tropospheric disturbances. To our knowledge, this transient wave contribution to the strengthening and deepening of the vortex has not been recognised before. The transient wave-2 reflection and corresponding wave-induced acceleration of the vortex is absent in the failed simulation (not shown). Together, Figures 4 and 5 indicate that the origin of these transient wave differences can be traced back to at least mid-November and the downward reflection is directly linked to poleward reflection from the subtropical USLM (Figure 4b). Thus, the diagnostics indicate that internal wave reflection in the USLM plays a key role in the strengthening and deepening of the vortex.

To better understand wave reflection in the USLM, and its linkage with the imposed winds in the equatorial USLM of the successful simulation, Figure 6 shows monthly-averaged cross-sections of quasi-geostrophic potential vorticity gradients $\bar{q}_\phi$ from the two simulations, with the TEM winds $\bar{v}*$ and $\bar{w}*$ superimposed as arrows. Both simulations show a localised region of strong positive

$\bar{q}_\phi$ over the Equator in the region 0.3–3 hPa and this is present throughout the period, as found in the climatological study of Hitchman and Huesmann (2007) (see their figures 1 and 2), who based their analysis on Ertel's PV. Regions of negative $\bar{q}_\phi$, associated with barotropic instability of the summer subtropical jet (Salby, 1981; Plumb, 1983; Limpasuvan and Leovy, 1995; Orsolini et al., 1997) are also evident from October onwards and the effect is more prevalent in the successful simulation by December/January. This is consistent with increased curvature of meridional winds in the subtropical USLM of the summer hemisphere, which is enhanced because of the stronger westerly SAO (see figure 3 of G2020). Greater meridional wind curvature implies a smaller horizontal component of PV gradient so that $\bar{q}_\phi$ is more likely to become zero. By October the $\bar{q}_\phi$ above ~0.5 hPa in the successful simulation has two well-separated maxima either side of the Equator at ~10–20°S and 20–30°N. This structure remains throughout the period and is consistent with increased mixing due to low-latitude Rossby wave breaking together with barotropic/inertial instability (Hitchman et al., 1987; Shuckburgh et al., 2001; Hitchman and Huesmann, 2007).

The positive $\bar{q}_\phi$ at ~20-30°N continues to strengthen and extend downward over time until by January there is a clear $\bar{q}_\phi$ maximum throughout the whole depth in the NH subtropical stratosphere, which is absent in the failed simulation. In January, this vertical strip of large positive $\bar{q}_\phi$ is accompanied by large positive values of
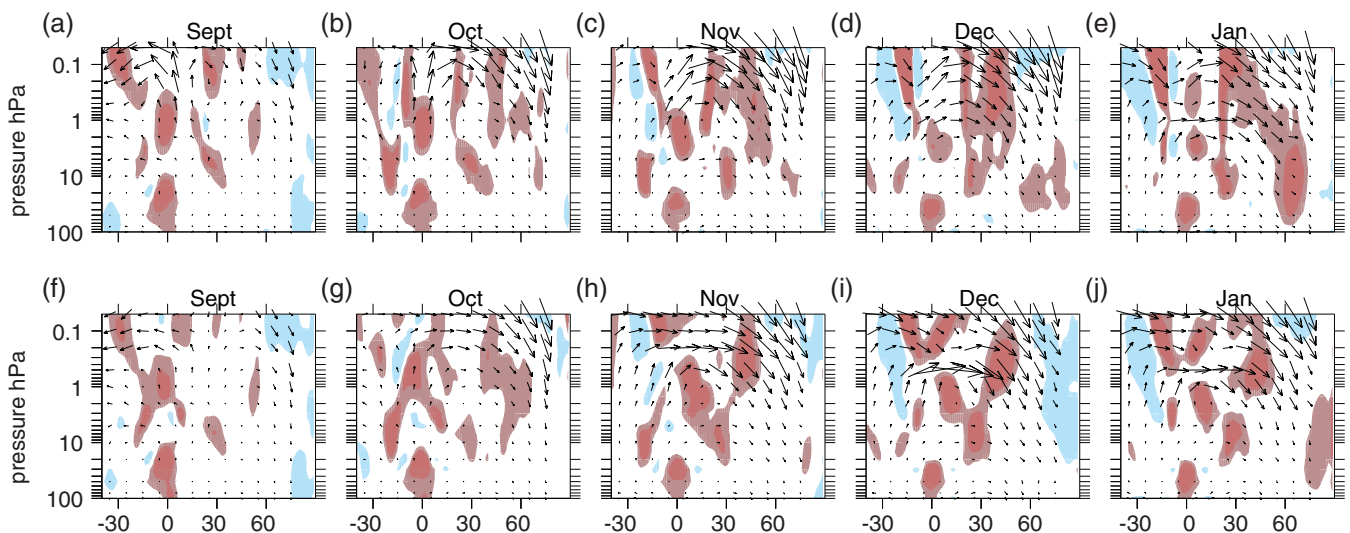
FIGURE 6 Latitude–height cross-sections (monthly, September 2008–January 2009) showing QGPV gradient (shaded regions; m·s⁻¹) from (a–e) the successful (AllTrop-UpStrat-Eq) simulation, (f–j) the failed (AllTrop) simulation. The QGPV gradients have been multiplied by the Earth's radius squared. Two shades of pink (contour values of 1,000 and 1,500) highlight regions with maximum positive values, shaded blue regions indicate regions with negative gradients. Overlaid on each plot are vector arrows showing the residual-mean circulation (m·s⁻¹; the vertical w* component has been scaled by 300 to aid visualization) [Colour figure can be viewed at wileyonlinelibrary.com]

$\overline{q}_\phi$ tracking along the polar vortex edge slanting equatorward with height from around 60°N up into the subtropical USLM. Together, they form a triangular structure of $\overline{q}_\phi$ in the winter stratosphere. A PV gradient structure with this formation has been previously identified as an important precondition for the SSW (Albers and Birner, 2014; see their figure 7). Here, we show that a good representation of the equatorial USLM winds is required in addition to the imposed tropospheric forcing to accurately reproduce this preconditioning feature, as well as its seasonal progression. We further suggest that the external resonance examined by Albers and Birner (2014) is closely related to the triangular structure of $\overline{q}_\phi$, a clear sign of nonlinear wave breaking (Killworth and McIntyre, 1985).

The development of the residual mean circulation is also clearly different between the two simulations. The residual mean circulation in the LM is stronger in the successful stimulation (compare e.g. September and October) with noticeably stronger upwelling near the Equator and increased northward outflow compared with the failed stimulation. Semeniuk and Shepherd (2001) and Tung and Kinnersley (2001) have noted that wave driving from the extratropical winter stratosphere close to the Equator is more likely to induce upwelling over the Equator. Tung and Kinnersley (2001) suggested that this enhanced stratospheric upwelling is most likely to be evident towards the end of winter, since the surf zone extends closer to the Equator by that time. However, the diagnostics from the successful simulation suggests that in 2008/2009 this effect occurs from early winter in the LM, with strong meridional transfer of wave activity starting from as early as October. The increased upwelling is thus additional evidence for the extension of wave breaking further into equatorial latitudes. Strong northward flow from the equatorial region where the winds are westerly is also consistent with enhanced synoptic-scale wave breaking (Hitchman et al., 1987; Shuckburgh et al., 2001; Hitchman and Huesmann, 2007). The diagnostics therefore suggest that the presence of localized Rossby wave breaking, in association with barotropic instability of the summer easterly jet and enhanced inertial instability during the westerly phase of the SAO, aids the development of nonlinear poleward wave reflection in the winter subtropical USLM. Nevertheless, the precise role of inertial/barotropic instability in triggering internal wave reflection is not well understood and requires further investigation.

In contrast, the residual mean circulation in the failed simulation is noticeably weaker above 0.5 hPa. In that simulation, the main feature of the circulation is a much stronger but shallow cross-equatorial flow that develops rapidly from November into December, consistent with the timing of the early December minor SSW. A sharp transition of the meridional winds over the equatorial USLM region from negative (southward) in September to positive (northward) in October is also evident, consistent with a rapid transition to SAO easterlies and development of the nose of easterlies from October above ~0.5 hPa in Figure 2. The earlier onset of the SAO easterlies at 0.3–1 hPa and stronger cross-equatorial flow evident in Figure 6h–j near 1 hPa are thus consistent with stronger wave absorption in the subtropical LM and the absence of poleward wave reflection in Figure 4e.

In summary, the diagnostics suggest that the equatorial USLM zonal winds that form the upper flank of the equinoctial SAO in the height region 0.1–0.5 hPa play an important role, not only by defining the initial shape of the polar vortex and thus influencing Rossby wave propagation, but also through internal transient wave reflection. The prolonged westerly winds in the equatorial lower mesosphere at 0.1–0.5 hPa in the successful simulation are the precursor to a vortex that strengthens progressively and penetrates deeper into the lower stratosphere over time as a result of nonlinear wave breaking and jet sharpening. In contrast, the easterly SAO bias in the failed simulation confines the wave forcing closer to the polar vortex so that the polar night jet weakens earlier, with a minor SSW occurring in early December, after which the flow evolution diverges substantially from reality.

Figure 7 shows a schematic of the early winter (~October/November) zonal wind and PV gradients in the lower mesosphere near 0.5 hPa for each of the simulations, to summarise the influential factors and to highlight their differences. In the successful simulation, strong westerlies in the equatorial lower mesosphere at 0.1–0.5 hPa result in an initial conical-shaped polar vortex in the USLM, which leads to a delayed or weakened wave mean-flow interaction due to reduced upward propagation of quasi-stationary propagating Rossby waves (Waugh and Dritschel, 1999). The polar vortex structure together with the localized wave-breaking near the Equator result in poleward reflection of transient waves in the subtropical USLM. The reflected finite-amplitude transient waves act to suppress baroclinic growth of quasi-stationary waves from below, which result in a further strengthening of the polar vortex. A persistently wide and strong polar vortex thus becomes more resilient to wave disturbances, delaying the occurrence of an SSW. In contrast, the failed simulation involves strong wave-breaking and absorption in the winter hemisphere as planetary waves propagating from the troposphere first meet their critical line instead of a turning surface. Also, the subtropical critical line moves rapidly into the winter hemisphere, confining wave forcing to the polar vortex, thus initiating an earlier onset of the SSW.

## Successful simulation
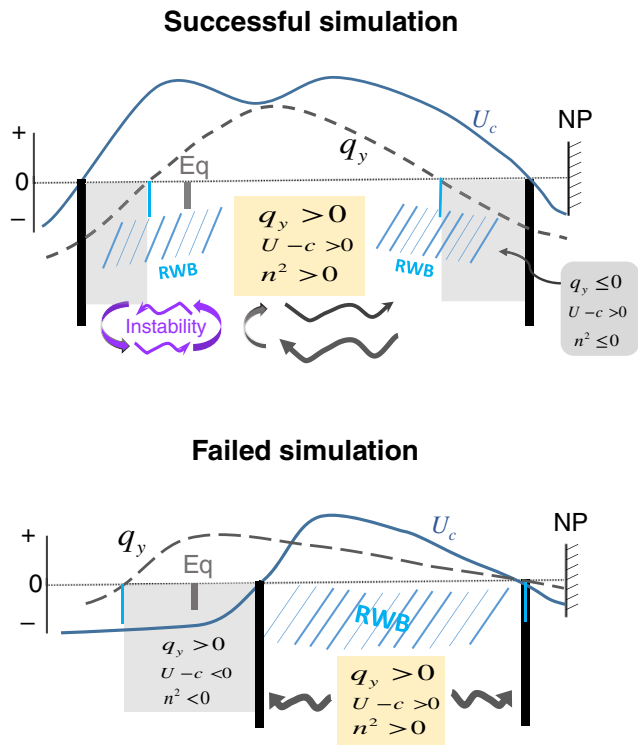
Failed simulation

FIGURE 7 A schematic description of the wave geometry for the successful and failed simulations in the USLM during early winter. The PV gradient q_y (dashed curve) and $U_c = U - C$ (solid curve) profiles are shown together with their zero points representing the critical lines (vertical thick black) and turning surfaces (vertical thin cyan bar), respectively. The plus and minus signs indicate positive and negative values of U_c and q_y at a given pressure level. Latitudinal regions of wave propagation are indicated by the yellow shaded box where refractive index n^2 is positive. Regions of wave evanescence are indicated by the grey shaded boxes where refractive index n^2 become negative. Dark grey arrows mark meridional Rossby wave propagation. Semi-circular grey arrow marks subtropical transient wave reflection. Purple arrows represent synoptic-scale wave breaking and mixing associated with barotropic instability of the summer easterly jet and inertial instability in association with the SAO westerly phase. Blue backslashes indicate Rossby wave breaking (RWB). The locations of Equator and North Pole are indicated by Eq and NP, respectively [Colour figure can be viewed at wileyonlinelibrary.com]

3.2 | SSW sensitivity to SAO transition timing: 1979–2018

While the diagnostics thus far indicate an influence of the LM westerly-to-easterly SAO transition on the 2008/2009 SSW, we question whether this was an unusual event or whether the influence is present in other years and could therefore be a useful tool in SSW prediction. G2020 performed case-studies of two additional winters (1988/1989 and 2005/2006) and found similar encouraging results. Accurate timing of the SSW in each winter was only
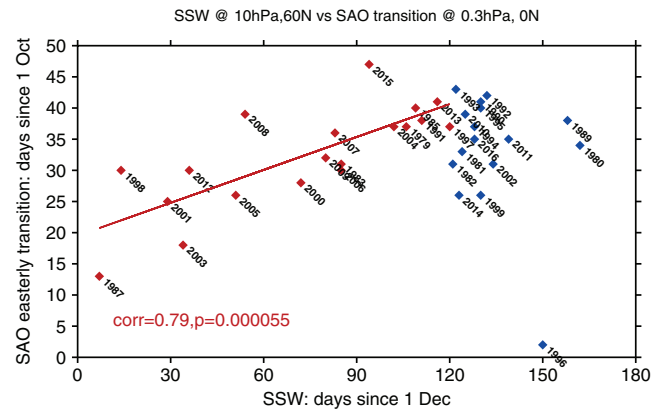
FIGURE 8 Scatter plot showing relationship between the date at which the ERA-I zonally averaged zonal winds at 60°N, 10 hPa reverses to easterly, indicating an SSW (*x*-axis; days since 1 December) and the date at which the equatorial zonally averaged zonal winds reverse to easterly at 0.29 hPa after 1 October, indicating the transition from westerly-to-easterly SAO phase (*y*-axis; days since 1 October). Red squares show SSWs in DJFM, blue squares show final warmings in April/May. The year associated with each square is the year at the start of winter for example, 1987 denotes the winter of 1987/1988. Red line shows the line of best fit to the red (mid-winter) SSW years, and the associated rank correlation and statistical significance is also shown. Three winters (1984/1985, 1986/1987 and 1988/1989) have been excluded due to unrealistic early SAO transitions [Colour figure can be viewed at wileyonlinelibrary.com]

achieved when the additional relaxation of the equatorial USLM zonal winds towards ERA-I was imposed (see G2020 supplementary information), suggesting that the SAO influence is present in other years.

To extend the G2020 analysis we investigate the relationship between SSW date and the SAO westerly-to-easterly transition date for all years in the period 1979–2018, using ERA-I data. The date of the SAO westerly-to-easterly transition was determined by identifying the transition date after 1 October when the equatorial winds at a selected USLM pressure level first reverse from westerly to easterly. Daily ERA-I data on model levels were used, to enable access to the upper-level data and to avoid loss of accuracy when data are interpolated from model levels to standard pressure levels. The SAO transition date was found to vary widely, from early October to mid-November. Similarly, the timing of the major SSWs was identified by determining when the zonally averaged zonal winds at 60°N, 10 hPa became easterly and remained easterly for at least 3 days. Once an SSW was identified, no further events were counted in that winter.

Figure 8 shows a scatter plot (red squares) between the SSW timing (*x*-axis; days since 1 December) and the westerly-to-easterly transition date at ~0.3 hPa (*y*-axis;

days since 1 October) for all years between 1979 and 2018. Three winters were excluded (1984/1985, 1986/1987, 1988/1989) because the westerly phase of the SAO was absent at ~0.3 hPa in those years. However, we note that years in which there was anomalous volcanic activity or extreme El Niño/Southern Oscillation (ENSO) years have not been excluded (this is common practice in many similar studies but substantially reduces the number of years). The scatter plot shows a high, statistically significant correlation ($r = 0.79$, $p < 0.01$) between the SSW date and the SAO westerly-to-easterly transition date. This relationship implies that an early SAO westerly-to-easterly phase transition date leads to an early SSW date while a late transition date leads to a delayed SSW in late winter. The correlation was found to maximise when the SAO transition at ~0.3 hPa was used but the correlation with the SAO transition at ~0.5 hPa is still relatively high and statistically significant (correlation $r = 0.55$, $p = 0.014$). The fact that this correlation is statistically significant even when anomalous ENSO years are included, suggests that this USLM influence associated with SAO transitioning is independent of the surface processes that are well known to influence upward wave propagation from the troposphere (such as ENSO). This statistically significant correlation between the timing of the SAO transition and the timing of SSWs does not, in itself, demonstrate causality since both could be a response to third-party forcing such as the timing and/or strength of planetary wave forcing from the troposphere. Nevertheless, the G2020 experiments that examine three different winters have clearly demonstrated that imposing the tropospheric wave forcing alone in those winters cannot reproduce the correct SSW timing, whilst additionally imposing the SAO zonal wind evolution achieved an accurate simulation. Extension of this correlation using data from 40 winters supports the hypothesis that the timing of SSWs depends on the SAO transition date as well as on the tropospheric wave forcing.

The analysis was also extended to April and May (blue squares), to include quiescent years with a stable vortex in which no mid-winter SSW occurred (the first identified transition to easterlies at 60°N, 10 hPa in April/May therefore indicates the final warming). Apart from 1996/1997, they all have relatively late SAO westerly-to-easterly transitions, consistent with an influence from the SAO even in those years. However, the correlation is reduced significantly ($r = 0.33$, $p < 0.05$), suggesting that other factors such as weak tropospheric wave forcing may have also been important in those years. Excluding the 1996/1997 winter increases the correlation to 0.44 ($p < 0.01$). We note that in 1996/1997 there was a near major SSW in late November/early December (the 60°N 10 hPa zonal winds reduced to ~3 m·s⁻¹) so this year may not be such an outlier as Figure 8 suggests. Similarly, the failed simulation of
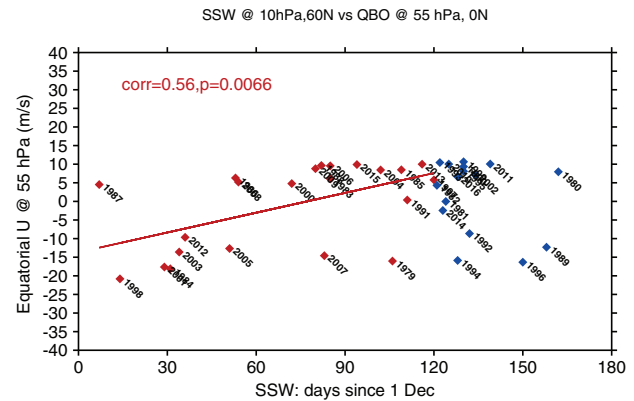
FIGURE 9 As Figure 8 but showing the relationship between SSW date (since 1 December) and amplitude of the QBO (m·s⁻¹) at 0°N, 55 hPa [Colour figure can be viewed at wileyonlinelibrary.com]

the 2008/2009 winter had a very early westerly-to-easterly transition but strictly, did not achieve a major SSW until February, since the 60°N 10 hPa zonally averaged zonal winds in early December SSW did not reduce to zero (Figure 1) and would strictly be classed as a minor SSW. This would place the failed simulation as a similar outlier on the Figure 8 correlation plot. Nevertheless, we have seen that the early December minor SSW was an important indicator of the subsequent winter flow evolution of that simulation.

The high correlation between SSW date and SAO westerly-to-easterly transition date can be compared with the well-known Holton–Tan relationship that links SSW occurrence with the QBO phase (Holton and Tan, 1980; 1982). Figure 9 shows a similar scatter plot of SSW timing against the QBO phase at 55 hPa in December (all years have been included in this scatter plot). The 55 hPa level in December was found to maximise the correlation. This is a lower level than the ~40 hPa level that Dunkerton *et al.* (1988) and other subsequent studies have usually employed. This is partly because we have included March SSWs in our analysis (and our analysis also covers more recent years).

The well-known early-winter Holton–Tan relationship is evident in December and January, with virtually no SSWs occurring in the QBO-W phase. Using the full December–March (DJFM) a statistically significant correlation of $r = 0.56$ ($p < 0.01$) is achieved and this increases to $r = 0.68$ ($p < 0.01$) for DJF-only. Nevertheless, we believe the inclusion of March is important since the number of mid-winter SSWs that have occurred in March is not negligible. Including April and May to take account of years with only final warming events serves to reduce the correlations further and they become insignificant.

Comparison of the DJFM correlations using the SAO westerly-to-easterly transition time (0.79) and the QBO

index (0.56) suggests that the SAO transition time may be a more reliable indicator of the subsequent timing of mid-winter SSWs than the QBO. However, the two indices are not independent since, for example, the Kelvin and gravity wave forcing of the westerly SAO phase is known to depend on the underlying equatorial zonal winds that are determined by the QBO (Garcia *et al.*, 1997). The month and pressure level of the SAO wind maxima shift depending on the phase of the quasi-biennial oscillation (QBO) at 10 hPa. Smith *et al.* (2017) found that during easterly QBO, the westerly maxima are shifted upward, are about $10 \, m \cdot s^{-1}$ stronger and occur approximately 1 month later than those during the westerly QBO phase. Nevertheless, the correlation between the SAO westerly-to-easterly transition date and December QBO winds at 55 hPa is not particularly high ($r = 0.38$, $p < 0.05$) which suggests that the SAO transition date is influenced by other possible factors. These could include the strength of the tropical wave forcing that influences the strength of the outgoing westerly SAO phase, the strength of midlatitude planetary wave driving that influences the timing of the Brewer–Dobson circulation reversal and hence the incoming easterly SAO phase and possibly the 11-year solar cycle that influences the local temperature and wind structure in the equatorial USLM.

4 | SUMMARY

Simulations of the early-winter precursor to the 2008/2009 split vortex SSW have been explored in detail, following the initial analysis of Gray *et al.* (2020). Two model simulations are compared, in terms of the development of the polar vortex and the corresponding wave forcing. In both simulations a relaxation towards the ERA-I tropospheric zonal wind fields was included, so that the tropospheric wave forcing was effectively specified. Additionally, in one of the simulations the equatorial zonal winds were additionally relaxed in the equatorial USLM (10°S–10°N, above 5 hPa). Only this simulation was able to successfully simulate the timing and spatial characteristics of the observed SSW (referred to as the successful simulation). The relaxation of winds in the equatorial USLM thus appears to have a significant influence on the SSW timing.

The nature of the USLM wind influence on SSW timing has been explored in detail and mechanisms related to the upper flank of the SAO in the LM are proposed. A prolonged westerly phase of the SAO in the region 0.1–0.5 hPa around the autumnal equinox was found to be a key factor. Without the equatorial USLM relaxation the failed simulation develops an easterly model bias in the height region of 0.1–0.5 hPa. The resulting early-onset of the easterly SAO phase influences the winter NH wave mean-flow

interaction so that the interaction occurs too early (from October) and is constrained too far poleward. As a result, planetary wave breaking and absorption are confined to the polar vortex region. This weakens the vortex and leads to an unrealistically strong minor SSW in early December, after which the vortex development becomes increasingly unrealistic.

The equatorial USLM zonal wind relaxation in the successful simulation, on the other hand, helps to delay the easterly onset of the SAO in the LM. The presence of SAO westerlies in the LM help to define a strong conical-shaped vortex which determines the subsequent wave mean-flow interactions. Quasi-stationary Rossby waves are able to penetrate further equatorward before breaking and transferring their momentum to the background flow. The resulting absence of wave dissipation at high latitudes allows the vortex to strengthen and extend deeper into the mid-stratosphere. Additionally, the successful simulation shows evidence of repeated poleward wave reflection of transient waves from the subtropics and downward propagation near the polar vortex edge. These sustained events are accompanied by a strengthening of the vortex winds. This nonlinear reflection thus additionally helps to precondition the SSW by strengthening and extending it into the lower stratosphere.

In summary, the study emphasises the role of the SAO in determining the early winter conical shape of the vortex. This enables Rossby wave penetration closer to the Equator, internal transient wave generation and internal nonlinear wave reflection. The analysis points to the importance of the timing of the SAO westerly-to-easterly phase transition on the upper flank of the SAO in the height region 0.1–0.5 hPa. Without the relaxation of the equatorial USLM winds towards the ERA-I reanalysis the model has an easterly bias in this height region, in common with other models, so that the transition from westerly to easterly winds at 0.1–0.5 hPa occurs too early. As a result, the early-winter upward propagating Rossby waves encounter their critical surfaces in the USLM NH subtropics from early winter, which results in increased wave mean-flow interaction and the early disruption of the polar vortex.

The study suggests that improved representation of the USLM equatorial winds could lead to better forecasts of SSWs. However, further analysis to confirm the veracity of the identified SAO–SSW correlation using observational satellite data and other reanalysis datasets would be valuable since there is much uncertainty in the accuracy of wind data in the USLM (Fujiwara *et al.*, 2017; Smith *et al.*, 2020). Further examination of the source of SAO variability would also be useful, for example to explore whether the variability in timing of the westerly-to-easterly SAO transition is primarily associated

with the strength of the westerly wave forcing (larger wave forcing would prolong the westerly phase) or whether it is associated with the incoming easterly phase and thus by variability in midlatitude planetary wave forcing. Improved understanding of this variability and further model validation would help point to ways in which the model bias can be corrected.

CONFLICT OF INTEREST
The authors declare no competing interests.

AUTHOR CONTRIBUTIONS
Lesley J. Gray: Conceptualization; formal analysis; investigation; methodology; project administration; software; supervision. **Hua Lu:** Formal analysis; investigation; methodology; software; writing – review and editing. **Matthew J. Brown:** Investigation; methodology; writing – review and editing. **Jeff Knight:** Conceptualization; methodology; software; writing – review and editing. **Martin Andrews:** Investigation; methodology; writing – review and editing.

DATA AVAILABILITY STATEMENT
All reanalysis data employed in the study are available from the relevant Reanalysis web-site (see Section 2 for details). Data from the model simulations and analysis code are available from the authors on request.

ORCID
Lesley J. Gray https://orcid.org/0000-0002-7803-9277
Hua Lu https://orcid.org/0000-0001-9485-5082
Matthew J. Brown https://orcid.org/0000-0003-1127-0279
Jeff R. Knight https://orcid.org/0000-0003-1868-0852
Martin B. Andrews https://orcid.org/0000-0003-3145-2264

REFERENCES
Albers, J.R. and Birner, T. (2014) Vortex preconditioning due to planetary and gravity waves prior to sudden stratospheric warmings. *Journal of Atmospheric Science*, 71, 4028–4054.

Andrews, D.G. (1987) On the interpretation of the Eliassen–Palm flux divergence. *Quarterly Journal of the Royal Meteorological Society*, 113(475), 323–338. https://doi.org/10.1002/qj.49711347518.

Andrews, D.G., Holton, J.R. and Leovy, C.B. (1987) *Middle Atmosphere Dynamics*. International Geophysics Series, Vol. 40. San Diego, CA: Academic Press.

Ayarzagüena, B., Langematz, U. and Serrano, E. (2011) Tropospheric forcing of the stratosphere: a comparative study of the two different major stratospheric warmings in 2009 and 2010. *Journal of Geophysical Research*, 116(D18), D18114. https://doi.org/10.1029/2010JD015023.

Baldwin, M.P., Gray, L.J., Dunkerton, T.J., Hamilton, K., Haynes, P.H., Randel, W.J., Holton, J.R., Alexander, M.J., Hirota, I., Horinouchi, T., Jones, D.B.A., Kinnersley, J.S., Marquardt, C., Sato, K. and Takahashi, M. (2001) The quasi-biennial oscillation. *Reviews of Geophysics*, 39, 179–229. https://doi.org/10.1029/1999RG000073.

Baldwin, M.P., Birner, T., Brasseur, G., Burrows, J., Butchart, N., Garcia, R., Geller, M., Gray, L.J., Hamilton, K., Harnik, N., Hegglin, M.I., Langematz, U., Robock, A., Sato, K. and Scaife, A.A. (2018) 100 years of progress in understanding the stratosphere and mesosphere: A century of progress in atmospheric and related sciences: celebrating the American Meteorological Society centennial, AMS. *Meteorological Monographs*, 59, 27.1–27.29. https://doi.org/10.1175/AMSMONOGRAPHS-D-19-0003.1.

Baldwin, M.P., Ayarzagüena, B., Birner, T., Butchart, N., Butler, A.H., Charlton-Perez, A.J., Domeisen, D.I.V., Garfinkel, C.I., Garny, H., Gerber, E.P., Hegglin, M.I., Langematz, U. and Pedatella, N.M. (2021) Sudden stratospheric warmings. *Reviews of Geophyics*, 59, e2020RG000708. https://doi.org/10.1029/2020RG000708.

Brunet, G. and Haynes, P.H. (1996) Low-latitude reflection of Rossby wave trains. *Journal of Atmospheric Sciences*, 53(3), 482–496.

Butler, A.H., Arribas, A., Athanassiadou, M., Baehr, J., Calvo, N., Charlton-Perez, A.J., Déqué, M., Domeisen, D.I.V., Fröhlich, K., Hendon, H., Imada, Y., Ishii, M., Iza, M., Karpechko, A.Y., Kumar, A., MacLachlan, C., Merryfield, W.J., Müller, W.A., O'Neill, A., Scaife, A.A., Scinocca, J., Sigmond, M., Stockdale, T.N. and Yasuda, T. (2016) The Climate-system Historical Forecast Project: do stratosphere-resolving models make better seasonal climate predictions in boreal winter? *Quarterly Journal of the Royal Meteorological Society*, 142(696), 1413–1427. https://doi.org/10.1002/qj.2743.

Butler, A.H., Sjoberg, J.P., Seidel, D.J. and Rosenlof, K. (2017) A sudden stratospheric warming compendium. *Earth System Science Data*, 9(1), 63–76. https://doi.org/10.5194/essd-9-63-2017.

Butler, A.H., Charlton-Perez, A.J., Domeisen, D.I.V., Garfinkel, C., Gerber, E.P., Hitchcock, P., Karpechko, A.Y., Maycock, A.C.,

Sigmond, M., Simpson, I. and Son, S.-W. (2018) Sub-seasonal predictability and the stratosphere. In: Robertson, A. and Vitart, F. (Eds.) *Sub-Seasonal to Seasonal Prediction: The gap between weather and climate forecasting*. Amsterdam, Netherlands: Elsevier, pp. 224–238.

Charlton, A.J. and Polvani, L.M. (2007) A new look at stratospheric sudden warmings. Part I: Climatology and modeling benchmarks. *Journal of Climate*, 20(3), 449–469.

Charlton-Perez, A.J., Ferranti, L. and Lee, R.W. (2018) The influence of the stratospheric state on North Atlantic weather regimes. *Quarterly Journal of the Royal Meteorological Society*, 144(713), 1140–1151.

Dimdore-Miles, O., Gray, L.J. and Osprey, S. (2021) Origins of multi-decadal variability in sudden stratospheric warmings. *Weather and Climate Dynamics*, 2, 205–231. https://doi.org/10.5194/wcd-2-205-2021.

Domeisen, D.I.V., Martius, O. and Jiménez-Esteve, B. (2018) Rossby wave propagation into the Northern Hemisphere stratosphere: the role of zonal phase speed. *Geophysical Research Letters*, 45, 2064–2071. https://doi.org/10.1002/2017GL076886.

Domeisen, D.I.V., Butler, A.H., Charlton-Perez, A.J., Ayarzagüena, B., Baldwin, M.P., Dunn-Sigouin, E., Furtado, J.C., Garfinkel, C.I., Hitchcock, P., Karpechko, A.Y., Kim, H., Knight, J., Lang, A.L., Lim, E.-P., Marshall, A., Roff, G., Schwartz, C., Simpson, I.R., Son, S.-W. and Taguchi, M. (2020) The role of the stratosphere in subseasonal to seasonal prediction: 2. Predictability arising from stratosphere–troposphere coupling. *Journal of Geophysical Research: Atmospheres*, 125(2), e2019JD030923. https://doi.org/10.1029/2019JD030923.

Dunkerton, T.J., Delisi, D.P. and Baldwin, M.P. (1988) Distribution of major stratospheric warmings in relation to the quasi-biennial oscillation. *Geophysical Research Letters*, 15(2), 136–139.

Fujiwara, M., Wright, J.S., Manney, G.L., Gray, L.J., Anstey, J., Birner, T., Davis, S., Gerber, E.P., Harvey, V.L., Hegglin, M.I., Homeyer, C.R., Knox, J.A., Krüger, K., Lambert, A., Long, C.S., Martineau, P., Molod, A., Monge-Sanz, B.M., Santee, M.L., Tegtmeier, S., Chabrillat, S., Tan, D.G.H., Jackson, D.R., Polavarapu, S., Compo, G.P., Dragani, R., Ebisuzaki, W., Harada, Y., Kobayashi, C., McCarty, W., Onogi, K., Pawson, S., Simmons, A., Wargan, K., Whitaker, J.S. and Zou, C.-Z. (2017) Introduction to the SPARC Reanalysis Intercomparison Project (S-RIP) and overview of the reanalysis systems. *Atmospheric Chemistry and Physics*, 17, 1417–1452. https://doi.org/10.5194/acp-17-1417-2017.

Garcia, R.R., Dunkerton, T.J., Lieberman, R.S. and Vincent, R.A. (1997) Climatology of the semiannual oscillation of the tropical middle atmosphere. *Journal of Geophysical Research*, 102(D22), 26019–26032.

Garfinkel, C.I., Schwartz, C., Domeisen, D.I.V., Son, S.-W., Butler, A.H. and White, I.P. (2018) Extratropical atmospheric predictability from the quasi-biennial oscillation in subseasonal forecast models. *Journal of Geophysical Research: Atmospheres*, 123, 7855–7866. https://doi.org/10.1029/2018JD028724.

Gray, L.J. (2003) The influence of the equatorial upper stratosphere on stratospheric sudden warmings. *Geophysical Research Letters*, 30(4), 1166. https://doi.org/10.1029/2002GL016430.

Gray, L.J. and Pyle, J.A. (1986) The semi-annual oscillation and equatorial tracer distributions. *Quarterly Journal of the Royal Meteorological Society*, 112(472), 387–407.

Gray, L.J., Phipps, S.J., Dunkerton, T.J., Baldwin, M.P., Drysdale, E.F. and Allen, M.R. (2001) A data study of the influence of the equatorial upper stratosphere on northern-hemisphere stratospheric sudden warnings. *Quarterly Journal of the Royal Meteorological Society*, 127(576), 1985–2003.

Gray, L.J., Crooks, S., Pascoe, C., Sparrow, S. and Palmer, M. (2004) Solar and QBO influences on the timing of stratospheric sudden warmings. *Journal of the Atmospheric Sciences*, 61, 2777–2796.

Gray, L.J., Brown, M., Knight, J.J., Andrews, M., Lu, H., O'Reilly, C. and Anstey, J. (2020) Forecasting extreme stratospheric polar vortex events. *Nature Communications*, 11, 4630.

Greer, K.R., Thayer, J.P. and Harvey, V.L. (2013) A climatology of polar winter stratopause warmings and associated planetary wave breaking. *Journal of Geophysical Research: Atmospheres*, 118, 4168–4180. https://doi.org/10.1002/jgrd.50289.

Harada, Y., Goto, A., Hasegawa, H., Fujikawa, N., Naoe, H. and Hirooka, T. (2010) A major stratospheric sudden warming event in January 2009. *Journal of the Atmospheric Sciences*, 67(6), 2052–2069.

Hartmann, D.L., Mechoso, C.R. and Yamazaki, K. (1984) Observation of wave-mean flow interaction in the Southern Hemisphere. *Journal of the Atmospheric Sciences*, 41, 351–362.

Harvey, V.L., Pierce, R.B., Fairlie, T.D. and Hitchman, M.H. (2002) A climatology of stratospheric polar vortices and anticyclones. *Journal of Geophysical Research*, 107(D20), 4442. https://doi.org/10.1029/2001JD001471.

Harvey, V.L., Randall, C.E., Goncharenko, L., Becker, E. and France, J. (2018) On the upward extension of the polar vortices into the mesosphere. *Journal of Geophysical Research: Atmospheres*, 123, 9171–9191. https://doi.org/10.1029/2018JD028815.

Hitchman, M.H. and Leovy, C.B. (1986) Evolution of the zonal mean state in the equatorial middle atmosphere during October 1978–May 1979. *Journal of the Atmospheric Sciences*, 43(24), 3159–3176. https://doi.org/10.1175/1520-0469(1986)043<3159:EOTZMS>2.0.CO;2.

Hitchman, M.H., Leovy, C.B., Gille, J.C. and Bailey, P.L. (1987) Quasi-stationary, zonally asymmetric circulations in the equatorial middle atmosphere. *Journal of the Atmospheric Sciences*, 44, 410–422.

Hitchman, M.H. and Huesmann, A.S. (2007) A seasonal climatology of Rossby wave breaking in the 320–2000-K layer. *Journal of the Atmospheric Sciences*, 64(6), 1922–1940. https://doi.org/10.1175/JAS3927.1.

Holton, J.R. and Tan, H.-C. (1980) The influence of the equatorial quasi-biennial oscillation on the global circulation at 50mb. *Journal of the Atmospheric Sciences*, 37, 2200–2208. https://doi.org/10.1175/1520-0469(1980)037,2200:TIOTEQ.2.0.CO;2.

Holton, J.R. and Tan, H.-C. (1982) The quasi-biennial oscillation in the Northern Hemisphere lower stratosphere. *Journal of the Meteorological Society of Japan*, 60, 140–148.

Ichimaru, T., Noguchi, S., Hirooka, T. and Mukougawa, H. (2016) Predictability changes of stratospheric circulations in Northern Hemisphere winter. *Journal of the Meteorological Society of Japan*, 94(1), 7–24. https://doi.org/10.2151/jmsj.2016-001.

James, I.N. and Gray, L.J. (1986) Concerning the effect of surface drag on the circulation of a baroclinic planetary atmosphere. *Quarterly Journal of the Royal Meteorological Society*, 112(474), 1231–1250.

James, I.N. (1987) Suppression of baroclinic instability in horizontally sheared flows. *Journal of the Atmospheric Sciences*, 44(24), 3710–3720.

Killworth, P.D. and McIntyre, M.E. (1985) Do Rossby-wave critical layers absorb, reflect or over-reflect? *Journal of Fluid Mechanics*, 161, 449–492.

Labitzke, K. (1982) On the interannual variability of the middle stratosphere during the northern winters. *Journal of the Meteorological Society of Japan*, 60, 124–139. https://doi.org/10.2151/jmsj1965.60.1_124.

Labitzke, K. and Kunze, M. (2009) On the remarkable Arctic winter in 2008/2009. *Journal of Geophysical Research*, 114(D1), D00102. https://doi.org/10.1029/2009JD012273.

Limpasuvan, V. and Leovy, C. (1995) Observation of the two-day wave near the southern summer stratopause. *Geophysical Research Letters*, 22(17), 2385–2388.

Lu, H., Baldwin, M.P., Gray, L.J. and Jarvis, M.J. (2008) Decadal-scale changes in the effect of the QBO on the northern stratospheric polar vortex. *Journal of Geophysical Research*, 113(D10), D10114. https://doi.org/10.1029/2007JD009647.

Lu, H., Bracegirdle, T.J., Phillips, T., Bushell, A. and Gray, L.J. (2014) Mechanisms for the Holton–Tan relationship and its decadal variation. *Journal of Geophysical Research: Atmospheres*, 119, 2811–2830.

Lu, H., Hitchman, M.H., Gray, L.J., Anstey, J.A. and Osprey, S.M. (2021a) On the role of Rossby wave breaking in the quasi-biennial modulation of the stratospheric polar vortex during boreal winter. *Quarterly Journal of the Royal Meteorological Society*, 146(729), 1939–1959. https://doi.org/10.1002/qj.3775.

Lu, H., Gray, L.J., Martineau, P., King, J.C. and Bracegirdle, T.J. (2021b) Regime behavior in the upper stratosphere as a precursor of stratosphere–troposphere coupling in the northern winter. *Journal of Climate*, 34(18), 7677–7696.

Manney, G.L., Schwartz, M.J., Krüger, K., Santee, M.L., Pawson, S., Lee, J.N., Daffer, W.H., Fuller, R.A. and Livesey, N.J. (2009) Aura Microwave Limb Sounder observations of dynamics and transport during the record-breaking 2009 Arctic stratospheric major warming. *Geophysical Research Letters*, 36, L12815. https://doi.org/10.1029/2009GL038586.

Matsuno, T. (1971) A dynamical model of the stratospheric sudden warming. *Journal of the Atmospheric Sciences*, 28, 1479–1494. https://doi.org/10.1175/1520-0469(1971)028<1479:ADMOTS>2.0.CO;2.

McIntyre, M.E. (1982) How well do we understand the dynamics of stratospheric warmings? *Journal of the Meteorological Society of Japan*, 60, 37–65. https://doi.org/10.2151/jmsj1965.60.1_37.

Mechoso, C.R., Hartmann, D.L. and Farrara, J. (1985) Climatology and interannual variability of wave, mean-flow interaction in the Southern Hemisphere. *Journal of the Atmospheric Sciences*, 42, 2189–2206.

Mukougawa, H., Hirooka, T. and Kuroda, Y. (2009) Influence of stratospheric circulation on the predictability of the tropospheric northern annular mode. *Geophysical Research Letters*, 36, L08814. https://doi.org/10.1029/2008GL037127.

Noguchi, S., Mukougawa, H., Kuroda, Y., Mizuta, R., Yabu, S. and Yoshimura, H. (2016) Predictability of the stratospheric polar vortex breakdown: an ensemble reforecast experiment for the splitting event in January 2009. *Journal of Geophysical Research: Atmospheres*, 121, 3388–3404. https://doi.org/10.1002/2015JD024581.

O'Neill, A. and Pope, V.D. (1988) Simulations of linear and nonlinear disturbances in the stratosphere. *Quarterly Journal of the Royal Meteorological Society*, 114(482), 1063–1110.

Orsolini, Y.J., Limpasuvan, V. and Leovy, C.B. (1997) The tropical stratopause in the UKMO stratospheric analyses: evidence for a 2-day wave and inertial circulations. *Quarterly Journal of the Royal Meteorological Society*, 123(542), 1707–1724.

Pascoe, C.L., Gray, L.J. and Scaife, A.A. (2006) A GCM study of the influence of equatorial winds on the timing of sudden stratospheric warmings. *Geophysical Research Letters*, 33, L06825.

Plumb, R.A. (1983) Baroclinic instability of the summer mesosphere: a mechanism for the quasi-two-day wave? *Journal of the Atmospheric Sciences*, 40, 262–270.

Robinson, W.A. (1986) The application of the quasi-geostrophic Eliassen–Palm flux to the analysis of stratospheric data. *Journal of the Atmospheric Sciences*, 43(10), 1017–1024.

Salby, M.L. (1981) The 2-day wave in the middle atmosphere: observations and theory. *Journal of Geophysical Research*, 86(10), 9654–9660. https://doi.org/10.1029/JC086iC10p09654.

Scaife, A.A., Knight, J.R., Vallis, G.K. and Folland, C.K. (2005) A stratospheric influence on the winter NAO and North Atlantic surface climate. *Geophysical Research Letters*, 32, L18715. https://doi.org/10.1029/2005GL023226.

Scaife, A.A., Karpechko, A.Y., Baldwin, M.P., Brookshaw, A., Butler, A.H., Eade, R., Gordon, M., MacLachlan, C., Martin, C., Dunstone, N. and Smith, D. (2016) Seasonal winter forecasts and the stratosphere. *Atmospheric Science Letters*, 17, 51–56.

Schneidereit, A., Peters, D.H.W., Grams, C.M., Quinting, J.F., Keller, J.H., Wolf, G., Teubler, F., Riemer, M. and Martius, O. (2017) Enhanced tropospheric wave forcing of two anticyclones in the prephase of the January 2009 major stratospheric sudden warming event. *Monthly Weather Review*, 145(5), 1797–1815.

Semeniuk, K. and Shepherd, T.G. (2001) Mechanism for tropical upwelling in the stratosphere. *Journal of the Atmospheric Sciences*, 58, 3097–3115.

Shuckburgh, E., Norton, W., Iwi, A. and Haynes, P. (2001) Influence of the quasi-biennial oscillation on isentropic transport and mixing in the tropics and subtropics. *Journal of Geophysical Research*, 106(D13), 14327–14337.

Sigmond, M., Scinocca, J.F., Kharin, V.V. and Shepherd, T.G. (2013) Enhanced seasonal forecast skill following stratospheric sudden warmings. *Nature Geoscience*, 6, 98–102.

Smith, A.K., Garcia, R.R., Moss, A.C. and Mitchell, N.J. (2017) The semiannual oscillation of the tropical zonal wind in the middle atmosphere derived from satellite geopotential height retrievals. *Journal of the Atmospheric Sciences*, 74, 2413–2425.

Smith, A.K., Holt, L.A., Garcia, R.R., Anstey, J.A., Serva, F., Butchart, N., Osprey, S., Bushell, A.C., Kawatani, Y., Kim, Y.-H., Lott, F., Braesicke, P., Cagnazzo, C., Chen, C.-C., Chun, H.-Y., Gray, L.J., Kerzenmacher, T., Naoe, H., Richter, J., Versick, S., Schenzinger, V., Watanabe, S. and Yoshida, K. (2022) The equatorial stratospheric semiannual oscillation and time-mean winds in QBOi models. *Quarterly Journal of the Royal Meteorological Society*, 148, 1593–1609. https://doi.org/10.1002/qj.3690.

Song, B.-G., Chun, H.-Y. and Song, I.S. (2020) Role of gravity waves in a vortex-split sudden stratospheric warming in January 2009. *Journal of the Atmospheric Sciences*, 77, 3321–3342. https://doi.org/10.1175/JAS-D-20-0039.1.

SPARC Reanalysis Intercomparison Project (S-RIP). (2022) Final report. In: Fujiwara, M., Manney, G.L., Gray, L.J. and Wright, J.S. (Eds.) SPARC Report No. 10, WCRP-6/2022. https://doi.org/10.17874/800dee57d13.

Telford, P.J., Braesicke, P., Morgenstern, O. and Pyle, J.A. (2008) Description and assessment of a nudged version of the new dynamics Unified Model. *Atmospheric Chemistry and Physics*, 8, 1701–1712.

Tripathi, O.P., Baldwin, M., Charlton-Perez, A.J., Charron, M., Eckermann, S.D., Gerber, E., Harrison, R.G., Jackson, D.R., Kim, B.-M., Kuroda, Y., Lang, A., Mahmood, S., Mizuta, R., Roff, G., Sigmond, M. and Son, S.-W. (2015) The predictability of the extratropical stratosphere on monthly time-scales and its impact on the skill of tropospheric forecasts. *Quarterly Journal of the Royal Meteorological Society*, 141(689), 987–1003.

Tripathi, O.P., Baldwin, M., Charlton-Perez, A.J., Charron, M., Cheung, J.C.H., Eckermann, S.D., Gerber, E., Jackson, D.R., Kuroda, Y., Lang, A., McLay, J., Mizuta, R., Reynolds, C., Roff, G., Sigmond, M., Son, S.-W. and Stockdale, T. (2016) Examining the predictability of the stratospheric sudden warming of January 2013 using multiple NWP systems. *Monthly Weather Review*, 144, 1935–1960.

Tung, K.-K. and Kinnersley, J.S. (2001) Mechanisms by which extra-tropical wave forcing in the winter stratosphere induces upwelling in the summer hemisphere. *Journal of Geophysical Research*, 106(D19), 22781–22791.

Waugh, D.W. and Dritschel, D.G. (1999) The dependence of Rossby wave breaking on the vertical structure of the polar vortex. *Journal of the Atmospheric Sciences*, 56(14), 2359–2375.

Walters, D., Baran, A.J., Boutle, I., Brooks, M., Earnshaw, P., Edwards, J., Furtado, K., Hill, P., Lock, A., Manners, J., Morcrette, C., Mulcahy, J., Sanchez, C., Smith, C., Stratton, R., Tennant, W., Tomassini, L., Van Weverberg, K., Vosper, S., Willett, M., Browse, J., Bushell, A., Carslaw, K., Dalvi, M., Essery, R., Gedney, N., Hardiman, S., Johnson, B., Johnson, C., Jones, A., Jones, C., Mann, G., Milton, S., Rumbold, H., Sellar, A., Ujiie, M., Whitall, M., Williams, K. and Zerroukat, M. (2019) The Met Office Unified Model Global Atmosphere 7.0/7.1 and JULES Global Land 7.0 configurations. *Geoscientific Model Development*, 12, 1909–1963.

Walker, C.C. and Magnusdottir, G. (2003) Nonlinear planetary wave reflection in an atmospheric GCM. *Journal of the Atmospheric Sciences*, 60(2), 279–286.